CHALMERS
FINITE ELEMENT CENTER

PREPRINT 2005–02

On the numerical modeling of quasi-static crack growth in linear elastic fracture mechanics

Per Heintz

Chalmers Finite Element Center
CHALMERS UNIVERSITY OF TECHNOLOGY
Göteborg Sweden 2005

CHALMERS FINITE ELEMENT CENTER

Preprint 2005–02

On the numerical modeling of quasi-static crack growth in linear elastic fracture mechanics

Per Heintz

CHALMERS

Chalmers Finite Element Center
Chalmers University of Technology
SE–412 96 Göteborg Sweden
Göteborg, March 2005

On the numerical modeling of quasi-static crack growth in linear elastic fracture mechanics
Per Heintz
NO 2005–02
ISSN 1404–4382

Chalmers Finite Element Center
Chalmers University of Technology
SE–412 96 Göteborg
Sweden
Telephone: +46 (0)31 772 1000
Fax: +46 (0)31 772 3595
www.phi.chalmers.se

Printed in Sweden
Chalmers University of Technology
Göteborg, Sweden 2005

ON THE NUMERICAL MODELING OF QUASI-STATIC CRACK GROWTH IN LINEAR ELASTIC FRACTURE MECHANICS

PER HEINTZ

Abstract. In this paper we present a strategy for the simulation of a propagating crack under mixed mode linear elastic conditions using a discontinuous finite element method. A key issue is to accurately compute the incremental change in the kink angle of the propagating crack during subsequent steps. We have chosen to work with a domain formulation of the material force vector as a criteria for the propagation direction. We describe the theoretical background together with the numerical implementation in detail and show some results for different loading conditions.

1. Introduction

In crack propagation simulations, one basic question is how to incorporate the discontinuity of the displacement field into the FE model. One straightforward method is to enforce mesh lines along the crack, *i.e.*, to create a new mesh at each propagation step as the crack propagates with time. A drawback with the re-meshing technique is the computational cost, since repeated re-meshing of the domain to obtain fitted meshes is costly. Other methods have been proposed in the literature to model discontinuities without any need for re-meshing. For instance, in the extended finite element method (XFEM) the approximation of the displacement field is enriched in the vicinity of the crack by incorporating additional basis functions using a partition of unity approach [12], see [13] and [14] for a description of the implementation.

In this paper we will use a discontinuous Galerkin method introduced in [6] and [8] by Hansbo and Hansbo. They proposed a new discontinuous finite element method for the simulation of strong and weak discontinuities in linear and nonlinear elasticity that allows for discontinuities internal to the elements in the approximation across the interface. They also showed optimal order of convergence in simple model cases.

In crack growth simulations, the accuracy of the crack path depends directly on the accuracy of the crack propagation and crack kinking criteria. In the paper by Bouchard et. al. [9] three different crack growth criteria and their prediction of the crack path for several test cases are compared: the maximal circumferential stress criterion, the strain energy density fracture criterion and the maximal strain energy release rate criterion. The maximal strain energy release rate criteria is the most complex method to implement

Date: March 3, 2005.

Key words and phrases. Crack propagation, discontinuous Galerkin, Nitsche's method, material forces.

Per Heintz, Department of Applied Mechanics, Chalmers University of Technology, S–412 96 Göteborg, Sweden, *email*: per.heintz@me.chalmers.se.

but seems to give the best results in their examples. In their paper a re-meshing of the computational domain is done at each propagating step.

We have chosen to use the concept of material, or configurational, forces as the crack kinking criteria. The material forces are fictious forces that corresponds to the change in potential energy with respect to a variation of the position of the defect. Due to the properties of this force, with a magnitude corresponding to the J-integral and a direction of maximum energy release, it seems natural to exploit its properties in a crack growth simulation. For recent developments in this field see the work by Maugin et. al [15], [16] who considers the elastic force on singularities and inhomogeneities. For a computational framework see the work by Steinmann et. al [3], [4] and Mueller [5]. For an error control algorithm for computing the material forces in linear elasticity, based on duality arguments, see [11].

2. Problem description

Let Ω be a bounded domain in $\Re^d,\ d=2,3$ with boundary $\partial\Omega = \partial\Omega^{\mathrm{D}} \cup \partial\Omega^{\mathrm{N}}$. We consider a linearly elastic specimen with an internal crack Γ^{C} that forms an interior boundary in Ω. For simplicity we will not consider the case in which we will have self contact between the parts in Ω separated by Γ^{C}. For the jump in the argument across an interface, here Γ^{C}, we use the notation $[\boldsymbol{w}] := \boldsymbol{w}^+ - \boldsymbol{w}^-$. Thus, we want to solve the following problem: find the displacement $\boldsymbol{u} = [u_i]_{i=1}^d$ and the symmetric stress tensor $\boldsymbol{\sigma} = [\sigma_{ij}]_{i,j=1}^d$ such that

$$\left\{ \begin{array}{rcl} -\nabla\cdot\boldsymbol{\sigma} &=& \boldsymbol{f} \quad \text{in } \Omega \\ \boldsymbol{\sigma} &=& \lambda(\nabla\cdot\boldsymbol{u})\boldsymbol{I} + 2\mu\boldsymbol{\varepsilon}(\boldsymbol{u}) \quad \text{in } \Omega \\ \boldsymbol{u} &=& \boldsymbol{g} \quad \text{on } \partial\Omega^{\mathrm{D}} \\ \boldsymbol{\sigma}\cdot\boldsymbol{n} &=& \boldsymbol{t} \quad \text{on } \partial\Omega^{\mathrm{N}} \end{array} \right. \tag{2.1}$$

where $\boldsymbol{f}$, $\boldsymbol{g}$, $\boldsymbol{t}$ and $\boldsymbol{n}$ are the body load, prescribed displacements, prescribed tractions and the outward pointing normal to $\partial\Omega$ respectively. λ and μ are the Lame material constants and $\boldsymbol{\varepsilon}$ is the symmetric strain tensor with components $\varepsilon_{ij} = \frac{1}{2}\left(\frac{\partial u_i}{\partial x_j} + \frac{\partial u_j}{\partial x_i}\right)$. Furthermore, $\boldsymbol{I}$ is the identity tensor with components $I_{ij} = 1$ if $i=j$ and $I_{ij} = 0$ if $i \neq j$. A straightforward way to solve (2.1) using the finite element method is to create a FE mesh in which Γ^{C} is taken into account for by letting an internal boundary of the mesh coincide with Γ^{C}. In a simulation where the crack moves with time it is thus necessary to create a new mesh fulfilling that condition at each crack increment. In the following sections we will explain how to circumvent this difficulty using the discontinuous Galerkin method introduced by Hansbo and Hansbo in [6] and [8]. Though there is nothing in principle precluding the use of the method in $\Re^3$, we will in this paper focus on the technically simpler 2D case.

3. The finite element method

Consider a subdivision $\mathcal{T}_h = \{K_i\}_{i=1,n_{el}}$ of a bounded domain Ω in $\Re^2$ with convex polygonal boundary $\partial\Omega$ consisting of n_{el} triangles with an internal polygonal interface (crack) Γ^{C} interior to Ω . Denote the set of triangles intersected by Γ^{C} by $G_h = \{K_i \in \mathcal{T}_h : K_i \cap \Gamma^{\mathrm{C}} \neq \emptyset\}$ see Figure 1. Since $\boldsymbol{u}$ is discontinuous over the interface Γ^{C} there is no relation

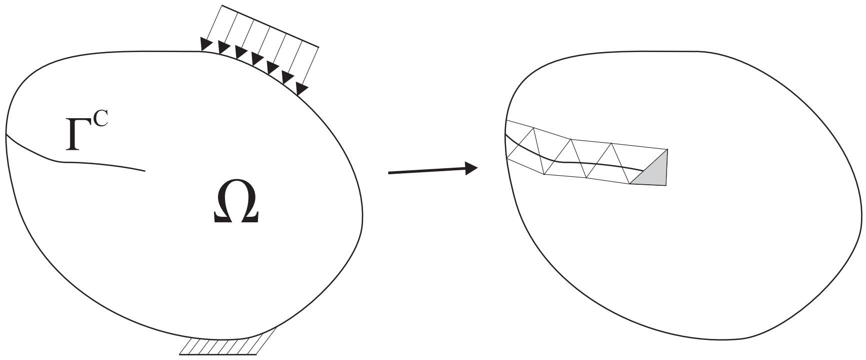

FIGURE 1. Left: The domain Ω with boundary conditions. Right: The FE mesh associated to G_h and the element ahead of the cracktip (shaded).

between the degrees of freedom associated with $\boldsymbol{u}^+$ and $\boldsymbol{u}^-$. In the section considering the implementation we will describe in detail how to create a FE mesh satisfying this condition. As to the continuity of the solution across the last cracked element and the element ahead of the cracktip (denoted Γ^{H}), see Figure 2, we use a Nitsche [10] term to glue the FE mesh together across Γ^{H}. Alternatively, the jump at the cracktip can be set identical to zero by changing the approximation as in Mergheim et. al [18].

The method reads: Find $\boldsymbol{u}_h \in V_h$ such that

$$a_N(\boldsymbol{u}_h, \boldsymbol{v}) = L(\boldsymbol{v}), \quad \forall \boldsymbol{v} \in V_h, \tag{3.1}$$

where

$$\begin{aligned} a_N(\boldsymbol{u}_h, \boldsymbol{v}) \;&=\; \int_\Omega \boldsymbol{\sigma}(\boldsymbol{u}_h) : \boldsymbol{\varepsilon}(\boldsymbol{v})\, dx - \int_{\Gamma^{\mathrm{H}}} \{\boldsymbol{\sigma}(\boldsymbol{u}_h)\cdot \boldsymbol{n}\}\cdot[\boldsymbol{v}]\, ds \\ &- \int_{\Gamma^{\mathrm{H}}} [\boldsymbol{u}_h]\cdot\{\boldsymbol{\sigma}(\boldsymbol{v})\cdot\boldsymbol{n}\}\, ds + \int_{\Gamma^{\mathrm{H}}} \frac{\delta}{h}[\boldsymbol{u}_h]\cdot[\boldsymbol{v}]\, ds \end{aligned} \tag{3.2}$$

and

$$L(\boldsymbol{v}) = \int_\Omega \boldsymbol{f}\cdot\boldsymbol{v}\, dx + \int_{\Gamma^{\mathrm{N}}} \boldsymbol{t}\cdot\boldsymbol{v}\, ds \tag{3.3}$$

As mentioned before, $[\boldsymbol{w}]$ represents the jump and $\{\boldsymbol{w}\}$ denotes a convex combination of the argument across the considered interface, *i.e.* $\{\boldsymbol{w}\} = \alpha\boldsymbol{w}^+ + (1-\alpha)\boldsymbol{w}^-$ with $\alpha \in [0,1]$ Thus, in (3.2), we use a mesh dependent penalty method with added terms involving the normal traction across Γ^{H} to enforce continuity across Γ^{H}. In contrast to the pure penalty method, *e.g.* without the terms involving the normal tractions across Γ^{H}, Nitsche's method is consistent and preserves the convergence rate for the underlying discretization. δ is a penalty like term that is chosen such that the discrete system is positive definite. The explicit values for δ and α is explained in the section considering the numerical examples. Moreover, h is a mesh dependent parameter that is defined as in [7] but it is possible to define the parameter different, for instance as the length of the edge, assuming a quasi-uniform mesh.

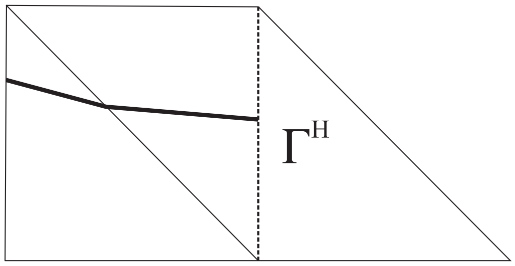

FIGURE 2. The cracktip intersects with Γ^{H} (dotted). The mesh is 'glued' across Γ^{H} using a Nitsche approach

4. The material forces in fracture mechanics

In the absence of material volume forces and inhomogeneities, the material (Newton-Eshelby) stress $\tilde{\boldsymbol{\Sigma}}$ is self-equilibrating

$$\nabla \cdot \tilde{\boldsymbol{\Sigma}} = \boldsymbol{0} \quad \text{in } \Omega \tag{4.1}$$

where the Newton-Eshelby stress is defined as

$$\tilde{\boldsymbol{\Sigma}} = W^{\mathrm{e}} \boldsymbol{I} - \boldsymbol{H}^{\mathrm{T}} \cdot \boldsymbol{\sigma} \tag{4.2}$$

In (4.2) W^{e} is the strain energy and $\boldsymbol{H}$ and $\boldsymbol{\sigma}$ are the displacement gradient tensor with components $H_{ij} = \frac{\partial u_i}{\partial x_j}$ and the Cauchy stress tensor, respectively. Consider now an arbitrary subdomain $A \subset \Omega$ with boundary Γ^{A} that surrounds the crack tip. We decompose Γ^{A} into its regular and singular parts, *i.e.*, $\Gamma^{A} = \Gamma^{r1} + \Gamma^{r2+} + \Gamma^{r2-} + \Gamma^{\mathrm{s}}$, see Figure 3. Starting from (4.1), we can single out the resultant material force acting on the crack tip from the associated weak format

$$F_{mat}(\boldsymbol{w}) = \int_{\Gamma^{\mathrm{r}}} (\tilde{\boldsymbol{\Sigma}} \cdot \boldsymbol{n}) \cdot \boldsymbol{w} \, ds - \int_{A} \boldsymbol{H}(\boldsymbol{w}) : \tilde{\boldsymbol{\Sigma}} \, dx \tag{4.3}$$

where F_{mat} is the material force associated to the test function $\boldsymbol{w}$, see [11]. The material force vector $\boldsymbol{F}_{mat}$, associated with the crack tip, is now obtained by using a $\boldsymbol{w}$ with first x_2-component equal to zero and then with x_1-component equal to zero. Alternatively, one can replace the virtual displacement vector $\boldsymbol{w}$ into a scalar function q, corresponding to testing in the two directions at the same time. For a straight traction free crack that is tested for a unit extension parallel to the cracktip we then recover the J-integral, see [11].

5. Implementation

At every step in the simulation process the following steps are carried out:

(1) Solve the governing equilibrium equations (2.1) using (3.1).
(2) Check if the crack propagation criteria are fulfilled and if so, compute the kink angle and the increment in crack length.
(3) Update the FE structures and proceed to step 1

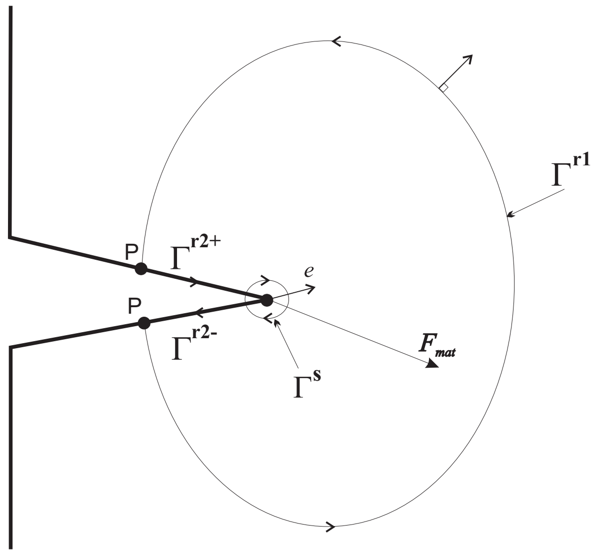

FIGURE 3. Subdomain with regular ($\Gamma^r = \Gamma^{r1} + \Gamma^{r2+} + \Gamma^{r2-}$) and singular Γ^{s} boundary.

For simplicity we will assume that the crack trajectory is well resolved by the mesh density and at each crack increment, we let the crack propagate through the whole element ahead of the cracktip.

5.1. **Crack propagation algorithm.** To handle the crack efficiently it is convenient to store some kind of data structure that defines the crack properly. We have chosen to keep track of the following data

(1) The crack polygon, *i.e.*, material coordinates of the crack where the crack polygon intersects with element boundaries.
(2) The elements that are cracked, *i.e.*, all $K \in G_h$.
(3) The mapping of new degrees of freedom, to be further specified below.

5.1.1. *Cutting elements and mapping degrees of freedom.* A crucial step is to handle the cracked elements properly such that new degrees of freedom are setup correctly. We will in the following section describe the process in detail for a linear approximation on triangles, the extension to higher order elements is straightforward using the same strategy. Assume that we are given a crack polygon consisting of a set of material coordinates $\boldsymbol{x}_c = \{\boldsymbol{x}_i\}_{i=1,n_c+1}$ where n_c is the number of cracked elements in the mesh, see Figure 4. We assume that the coordinates in $\boldsymbol{x}_c$ are ordered so that $\boldsymbol{x}_1$ defines the current position of the cracktip and $\boldsymbol{p}_i$ is the vector through element i in G_h starting from $\boldsymbol{x}_{i+1}$ and ending at $\boldsymbol{x}_i$. In case the crack is fully embedded in Ω and $x_{n_{c+1}}$ is also a cracktip coordinate the following strategy also holds.

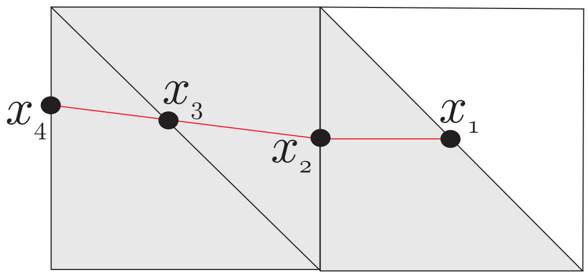

FIGURE 4. Small FE mesh with three cracked elements (shaded) and the corresponding crack polygon.

We now introduce a discontinuity over the crack polygon by splitting the shaded elements into two subelements, geometrically composed by a triangle and a quadrilateral, as follows. For each $K \in G_h$ (loop over index i)

(1) Extract the degrees of freedom and the associated material coordinates for the current cracked element.
(2) For each vertex v_j, $j = 1, n_{elementdofs}$ in the current element, with the associated material coordinates $\boldsymbol{x}_{v,j}$, decide if the vertex v_j lies to the left or to the right of the vector $\boldsymbol{p}_i$ by computing the signed area as follows. Define the vector $\boldsymbol{r}_j = \boldsymbol{x}_{v,j} - \boldsymbol{x}_{i+1}$ and compute $a(j) = \frac{1}{2}(\boldsymbol{p} \perp \boldsymbol{r})$ where
$$\boldsymbol{v} \perp \boldsymbol{w} = \begin{vmatrix} v_1 & w_1 \\ v_2 & w_2 \end{vmatrix}$$
   - $a(j) > 0.0$, v_j is to the left of the vector $\boldsymbol{p}_i$.
   - $a(j) < 0.0$, v_j is to the right of the vector $\boldsymbol{p}_i$.
   - $a(j) = 0.0$, v_j is parallel to the vector $\boldsymbol{p}_i$.
(3) Introduce new degrees of freedom associated with the vertex that have not already been taken care of (if $i = 1$, three vertices have to be considered).
(4) Finally, setup new degrees of freedom for the two subelements such that the continuity is preserved on both sides of the interface using the new degrees of freedom and the degrees of freedom for previously cracked elements.

The final result can be seen in Figure 5 where we have introduced new degrees of freedom at the cracked element vertices (denoted with i, j, k, l, m). The filled blacked vertices are those where continuity is preserved whereas the black circles corresponds to the degrees of freedom that must be created in order to obtain a linear approximation on each subelement. Thus, each cracked element has got twice as many degrees of freedom as an uncracked element.

5.1.2. *The assembly process.* The assembly process is carried out in three steps. First, we integrate the elements $K \in \Omega \setminus G_h$ using the proper quadrature for the element approximation order. Next, we integrate the stiffness associated with elements $K \in G_h$ as follows. For each $K \in G_h$ we have already subdivided the cracked element into two disjoint parts

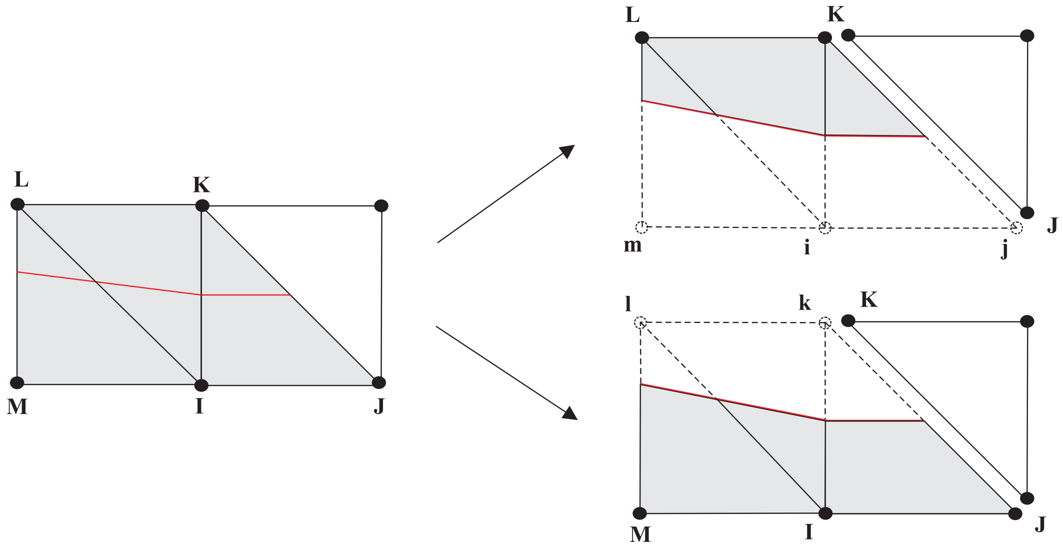

FIGURE 5. The final result obtained after splitting the elements and introducing new degrees of freedom.

K_1 and K_2, see Figure 6. The element stiffness associated with each cracked element is thus assembled in two steps. For linear elements we simply multiply the subarea with the basis functions evaluated at the geometrical midpoint. For higher order elements it is convenient to use a quadrature rule and the integration is carried out based on the quadrature points and weights associated with the chosen quadrature rule.

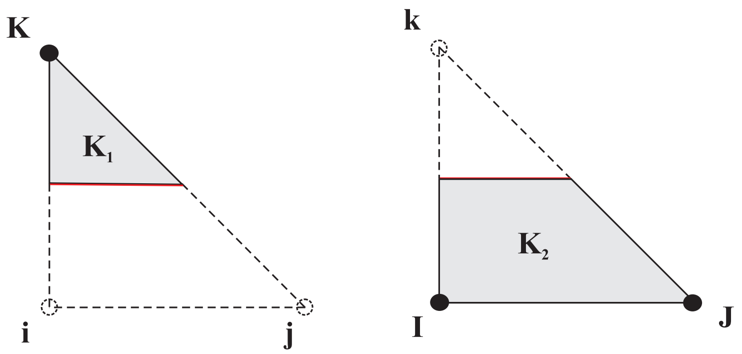

FIGURE 6. Quadrature on subelements

Remark: The FE approximation still relies on the initial triangulation and the geometrical subelement will only influence the choice of quadrature rule. The geometrical subelements can be 3 triangles and/or 1 triangle and 1 quad.

Finally, in order to obtain a continuous solution between the last cracked element and the element ahead of the cracktip we use a standard approach due to Nitsche (3.1) to glue the mesh together across Γ_{H}, as mentioned earlier.

5.1.3. *Evaluation of the direction of crack propagation.* After each solution step the crack growth criteria and, if the crack should propagate, the kink angle must be determined.

Due to the discontinuity some care has to be taken in order to compute the material force accurately. In the finite element setting we choose the subdomain A to coincide with a few elements around the cracktip. We then choose the scalar function such that $q(\boldsymbol{x}) = q_h(\boldsymbol{x}) = \Sigma_n q^n N^n(\boldsymbol{x})$, where N^n is the basis function associated with the node at $\boldsymbol{x} = \boldsymbol{x}_n$. Hence, we obtain

$$\boldsymbol{F}^n_{mat} = \int_{\Gamma^{r2+} \cup \Gamma^{r2-}} (\tilde{\boldsymbol{\Sigma}} \cdot \boldsymbol{n}) q \, ds - \int_A \boldsymbol{H}(q) : \tilde{\boldsymbol{\Sigma}} \, dx \tag{5.1}$$

Here, we let $q(\boldsymbol{x}) = 1$ in a small neighborhood of the cracktip and let q decay within the chosen domain until $q = 0$ at Γ^{r_1}.

The scalar function q associated with the chosen subdomain must be re-defined at each

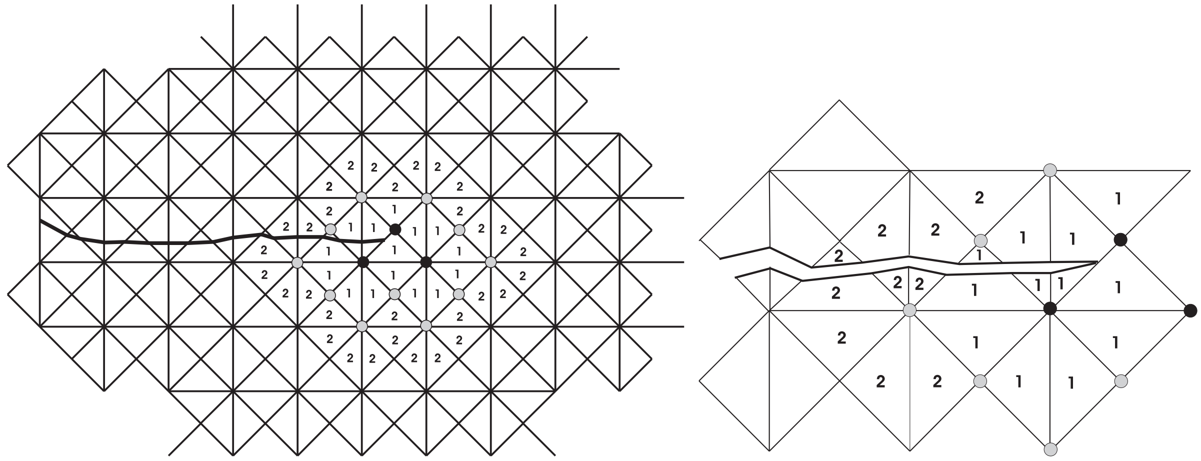

FIGURE 7. Element indicators for the integration

step since the subdomain moves with the cracktip. To handle the moving subdomain we use the following strategy:

1. The nodes of the element ahead of the cracktip (marked with filled black circles in Figure 7) are found.
2. The neighboring elements that support these nodes are marked with indicator 1. Within these elements we keep q constant.
3. The next layer of neighboring nodes (marked with filled grey circles) are found
4. The neighboring elements that supports these nodes, but are not already labeled with indicator 1, are marked with indicator 2. Within this layer we let q decay to zero.

The final result can be seen in Figure 7. Thus, for an efficient computation it is necessary to have the coupling between neighboring nodes in the computational mesh. However, since this information is also used for the graph of the sparse coefficient matrix there is no extra work. Alternatively, a similar approach can be used if only the element to element neighboring information is at hand.

An obvious difference compared to the J-integral is that the contribution from the crack faces cannot be neglected in case the crack faces is not parallel to the anticipated direction of crack extension. Since the purpose is to have no pre-defined direction of crackgrowth we always compute the contribution from the crack faces.

5.1.4. *Crack increment.* The final step is to propagate the crack through the element ahead of the cracktip given a (normalized) direction of crack extension r.

(1) Compute the point of intersection (x_1) between the vector $C \cdot r$ and the edges of the triangle. C is a simple scaling factor such that there is an intersection.
(2) Update the crack data structure.

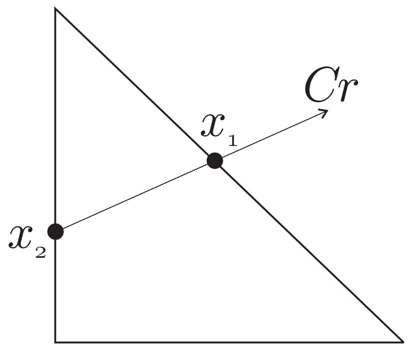

FIGURE 8. The intersection between the former cracktip x_2 and the new cracktip x_1.

1

6. Numerical examples

In this section we present three numerical examples that demonstrate the crack propagation algorithm, implemented as described in the previous sections. First, we consider a simple model problem of a single edged crack for which we compute and compare the energy release rate with the analytical value. Secondly, a weak and a stiff inclusion problem are considered. The final example demonstrates a more complicated loading case, taken from the litterature, where a simply supported beam is subjected to a pointload.

In all examples, the parameter α is chosen such that the normal tractions are evaluated from the uncracked element ahead of the cracktip. The parameter δ must be chosen high enough to ensure stability of the method. In all examples δ was set to $\delta = C \cdot (2\mu + 3\lambda)$ where C depends on the approximation order of the basis functions. For linear triangles $C = 2$ was sufficient in all examples. If the material properties are different between the last cracked element and the element ahead of the cracktip, we simply use the highest value obtained from the two different materials. For an in depth discussion and mathematical proofs concerning the choice of the parameter δ see [6], [8] and references therein. The elastic properties are given in terms of Youngs modulus E and poissons ratio ν and we use the relations

$$\lambda = \frac{E\nu}{(1+\nu)(1-2\nu)} \tag{6.1}$$

$$\lambda = \frac{E\nu}{1-\nu^2} \tag{6.2}$$

$$\mu = \frac{E}{2(1+\nu)} \tag{6.3}$$

where (6.1) and (6.2) are for plane strain and plain stress problems respectivily.

In example 2 and 3 we use a simple mesh refinement algorithm to increase the accuracy of the computed kink angle. The elements that are marked with indicator 1, see Figure 7, are subdivided into four new triangles in two steps. Thus the original elements with indicator 1 are subdivided into 16 new triangles. Due to the properties of the refinement algorithm, the refinement is diffused through the grid such that no hanging nodes and no sharp corners are obtained.

6.1. **Single edged crack.** Consider the single edged crack in Figure 9 subjected to a modus I load with $\boldsymbol{n} \cdot \boldsymbol{\sigma} \cdot \boldsymbol{n} = \sigma_0 = 1$. The body is in plane stress and the elastic parameters are $E = 1.0$ Pa and $\nu = 0.3$. The dimensions of the body are $W = 1.0$ m and $h = 2.0$ m. The stress intensity factor K_{I}, representing the strength of the singularity at the cracktip, is now obtained from

$$K_{\mathrm{I}} = \sqrt{\pi a} \cdot f(a, W), \tag{6.4}$$

where $f(a, W)$ is a geometry factor. The relation between the stress intensity and the energy release rate is

$$J = \frac{K_{\mathrm{I}}^2}{E} \tag{6.5}$$

The crack is initiated at $\boldsymbol{x} = (0.0, 1.0)$ and the initial crack length is set to $a = 0.125$ m. The energy release rate is evaluated, *i.e.* the material force vector projected in the direction parallel to the crack, at each crack propagation step. In this example we consider a straight traction free crack, thus $\boldsymbol{\sigma} \cdot \boldsymbol{n} = \mathbf{0}$ on $\Gamma^{r2+} \cup \Gamma^{r2-}$ and the contribution to the energy release rate from the crack faces vanishes since the normal vector of the crack faces is perpendicular to the anticipated direction of crack extension.

The results can be found in Figure 10 where the crack length a is plotted against the analytic and computed value of the energy release rate from eq. (6.4) and (6.5).

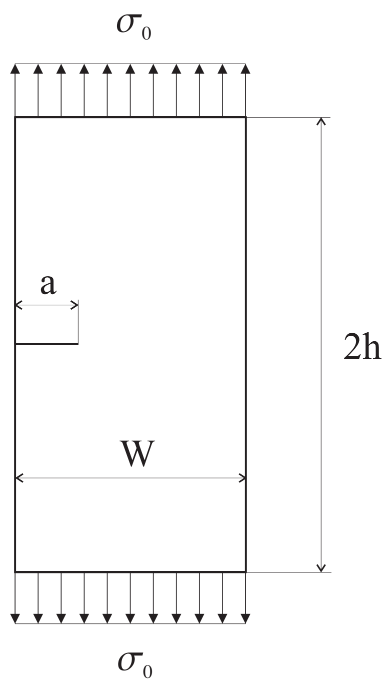

FIGURE 9. A single edged crack subjected to a modus I load.

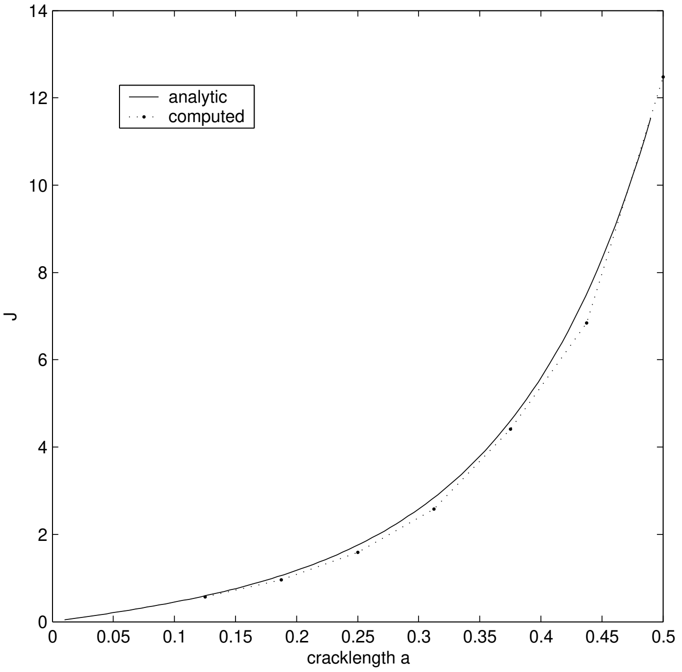

FIGURE 10. The computed value compared with the analytical value for the energy release rate at crackgrowth.

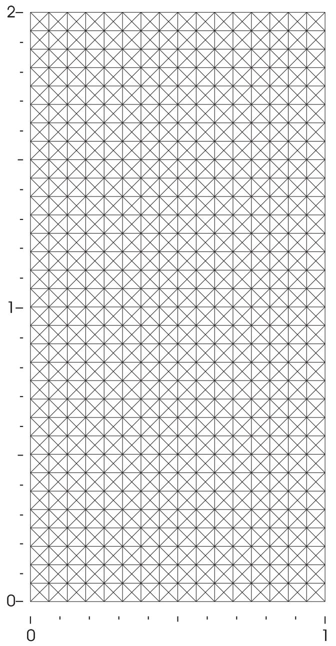

FIGURE 11. The computational mesh for example 1.

6.2. **Stiff vs weak inclusion.** As before, the single edge crack is initiated at the left boundary and a weak (or stiff) inclusion with radius 0.1m is inserted at $\boldsymbol{x} = (0.75, 1.0)$ m. The dimensions of the body are the same as in example 1 with $W = 1.0$ m and $h = 2.0$ m. The elastic modulus of the bulk body was set to $E = 1000$ Pa, the weak inclusion to $E = 1$ Pa and the stiff inclusion to $E = 1000000$ Pa. The resulting crack trajectories can be seen in Figure 12 and Figure 13. As seen in the figures, the crack tends towards the weak inclusion and away from the stiff inclusion.

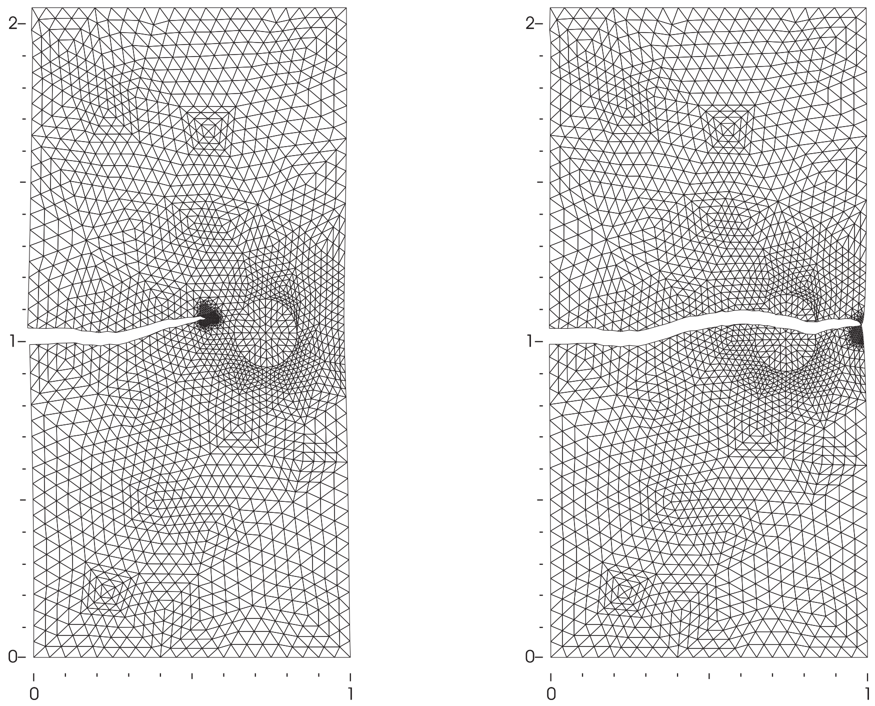

FIGURE 12. Crack trajectory for the weak inclusion.

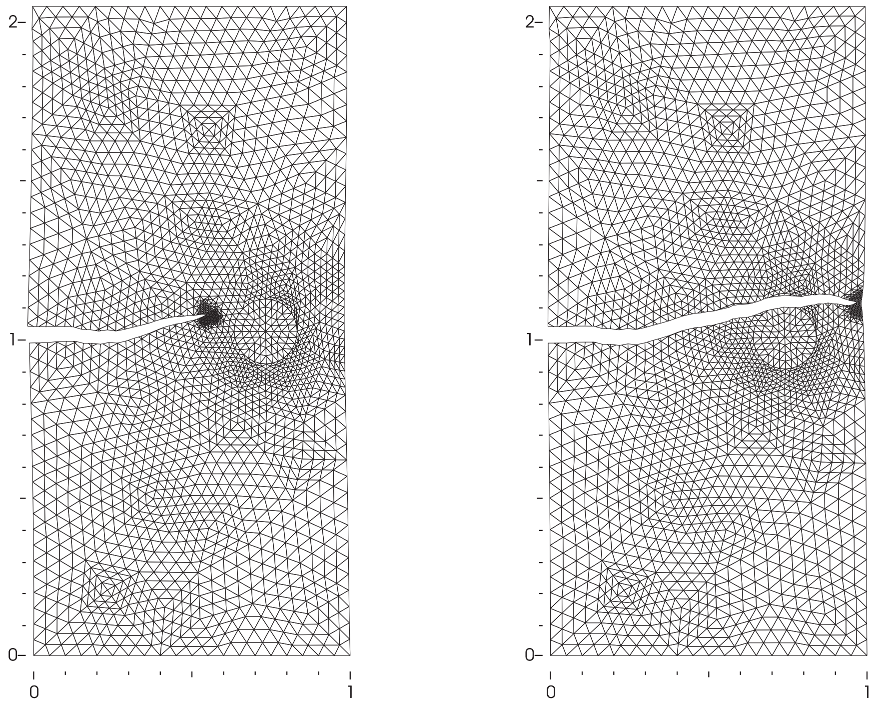

FIGURE 13. Crack trajectory for the stiff inclusion.

6.3. **Mixed mode conditions.** The described strategy is applied to model the propagation of a crack initiated at the lower boundary of a beam, see Figure 14. The three holes disturb the stress/strain field and give rise to curvilinear crack trajectories. This problem has also been used by other researchers, see [1] and [2], who compared their computational results with experiments. The crack paths were found to be highly dependent on the position of the initial crack. Therefore two different initial configurations were selected for the two examples considered here. The plate is simply supported near the lower corners and subjected to a concentrated load at the center of the upper edge. As in example 1, the material parameters where set to $E = 1$ and $\nu = 0.3$. A pointload $\boldsymbol{P} = (0, -1)$ was applied at the center of the upper boundary.

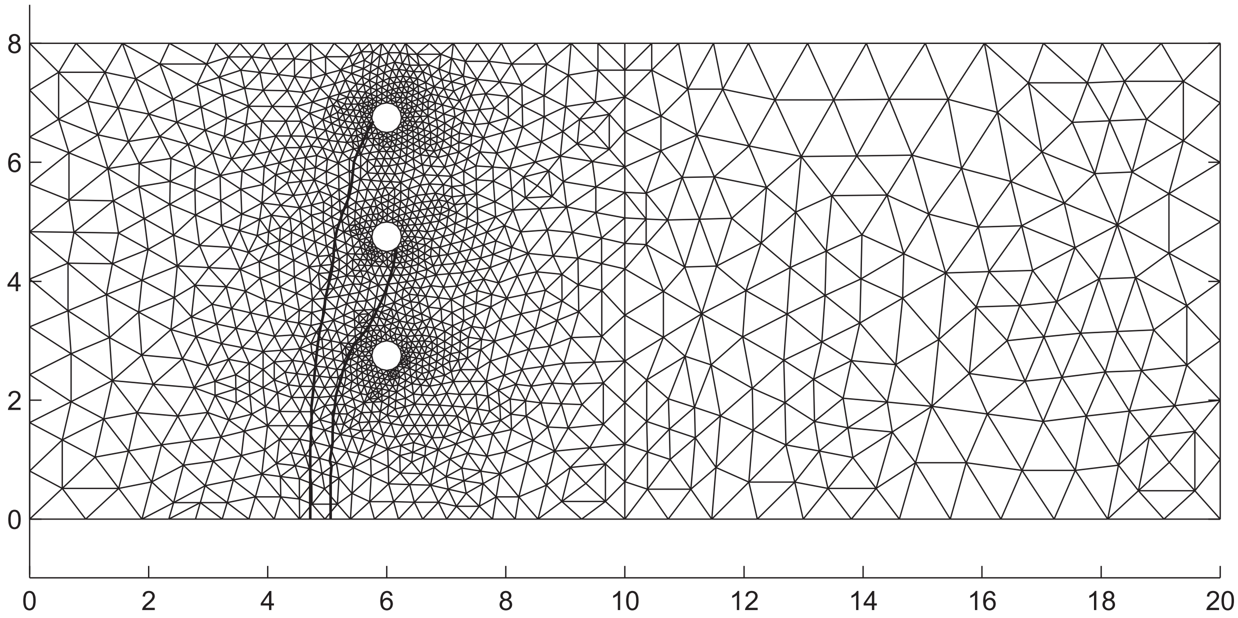

FIGURE 14. Crack propagation trajectories for two different starting positions of the crack

Figure 14 shows the crack trajectories for two different starting positions of the crack. The crack was initiated as a straight line cutting through five elemets before the simulation started. The trajectories shows similar results as in [2]. However, the material parameters in their paper was not presented.

7. Concluding remarks and outlook

In this paper we have presented a FE method for the simulation of a propagating crack under linear elastic conditions. We have described the implementation of the method in detail and presented two model problems where the strategy seems to give accurate results. The next step would be to incorporate a mixed FE method for the approximation of the traction, *i.e.*, contact (normal traction) and friction (tangential traction) between the crack faces. The mathematical framework for incorporating a cohesive zone model has already been considered by Hansbo and Hansbo in [8] where debonding of the interface, using a linear elastic spring-type model, was implemented. For related work we also refer to Mergheim et. al [18].

References

[1] S. Phongthanapanich, P. Dechaumphai. Adaptive Delaunay triangulation with object-oriented programming for crack propagation analysis. *Finite Elements in Analysis and Design* 2004; **40**:1753–1771

[2] T. N. Bittencourt, P. A. Wawrzynek, A. R. Ingraffea. Quasi-automatic simulation of crack propagation for 2D LEFM problems. *Engineering Fracture Mechanics* 1996;**55**:321–334.

[3] P. Steinmann. Application of Material Forces to Hyperelastostatic Fracture Mechanics. Part I: Continuum mechanical setting. *International Journal of Solids and Structures* 2000; **37**:7371–7391.

[4] P. Steinmann, D. Ackermann, F. J. Barth. Application of Material Forces to Hyperelastostatic Fracture Mechanics. Part II: Computational setting. *International Journal of Solids and Structures* 2001; **38**:5509–5526.

[5] R. Mueller, S. Kolling and D. Gross On configurational forces in the context of the finite element method *International Journal for Numerical Methods in engineering* 2002; **53**:1557–1574

[6] A. Hansbo, P. Hansbo. An unfitted finite element method, based on Nitsche's method, for elliptic interface problems. *Computer methods in applied mechanics and engineering* 2002; **191**:5537–5552

[7] P. Hansbo, M.G. Larson. Discontinuous Galerkin methods for incompressible and nearly incompressible elasticity by Nitsche's method. *Computer methods in applied mechanics and engineering* 2002; **191**:1895–1908

[8] A. Hansbo, P. Hansbo. A finite element method for the simulation of strong and weak discontinuities in solid mechanics. *Computer methods in applied mechanics and engineering* 2004; **193**:3523–3540

[9] P. O. Bouchard, F. Bay, Y. Chastel Numerical modeling of crack propagation: automatic remeshing and comparison of different criteria. *Computer methods in applied mechanics and engineering* 2003; **192**:3887–3908

[10] J. Nitsche *Über ein Variationsprinzip zur Lösung von Dirichlet-Problemen bei Verwendung von Teilräumen, die keinen Randbedingungen unterworfen sind.* Abh. Math. Sem. Univ. Hamburh, 36 (1971), pp9-15

[11] P. Heintz, F. Larsson, P. Hansbo, K. Runesson Adaptive strategies and error control for comptuting material forces in fracture mechanics *International journal for numerical Methods in Engineering* 2004;(**60**):1287–1299

[12] I. Babuska The partition of unity method *International journal for numerical methods in engineering* 40 727–758 (1997)

[13] N. Sukumar, J.-H. Prvost Modeling quasi-static crack growth with the extended finite element method *International Journal of Solids and Structures* 40 (2003) 7513–7537

[14] R. Huang, N. Sukumar, J.-H. Prvost Modeling quasi-static crack growth with the extended finite element method. Part II: Numerical applications *International Journal of Solids and Structures* 40 (2003) 7539–7552

[15] G.A. Maugin *Material Inhomogeneities in Elasticity.* Chapman & Hall; London, 1993.

[16] G.A. Maugin Material forces: Concepts and applications. *Applied Mechanics Reviews*, **48**:213–245, 1995
[17] J.D. Eshelby *The force on an elastic singularity* Philosophical Transactions of the Royal Society of London, A244:1–17, 1951
[18] J. Mergheim, E. Kuhl, P. Steinmann A finite element method for the computational modelling of cohesive cracks *International journal for numerical methods in engineering* (in press)

Chalmers Finite Element Center Preprints

2003–01	*A hybrid method for elastic waves* Larisa Beilina
2003–02	*Application of the local nonobtuse tetrahedral refinement techniques near Fichera-like corners* L. Beilina, S. Korotov and M. Křížek
2003–03	*Nitsche's method for coupling non-matching meshes in fluid-structure vibration problems* Peter Hansbo and Joakim Hermansson
2003–04	*Crouzeix–Raviart and Raviart–Thomas elements for acoustic fluid–structure interaction* Joakim Hermansson
2003–05	*Smoothing properties and approximation of time derivatives in multistep backward difference methods for linear parabolic equations* Yubin Yan
2003–06	*Postprocessing the finite element method for semilinear parabolic problems* Yubin Yan
2003–07	*The finite element method for a linear stochastic parabolic partial differential equation driven by additive noise* Yubin Yan
2003–08	*A finite element method for a nonlinear stochastic parabolic equation* Yubin Yan
2003–09	*A finite element method for the simulation of strong and weak discontinuities in elasticity* Anita Hansbo and Peter Hansbo
2003–10	*Generalized Green's functions and the effective domain of influence* Donald Estep, Michael Holst, and Mats G. Larson
2003–11	*Adaptive finite element/difference method for inverse elastic scattering waves* Larisa Beilina
2003–12	*A Lagrange multiplier method for the finite element solution of elliptic domain decomposition problems using non-matching meshes* Peter Hansbo, Carlo Lovadina, Ilaria Perugia, and Giancarlo Sangalli
2003–13	*A reduced P^1–discontinuous Galerkin method* R. Becker, E. Burman, P. Hansbo, and M.G. Larson
2003–14	*Nitsche's method combined with space–time finite elements for ALE fluid–structure interaction problems* Peter Hansbo, Joakim Hermansson, and Thomas Svedberg
2003–15	*Stabilized Crouzeix–Raviart element for the Darcy-Stokes problem* Erik Burman and Peter Hansbo
2003–16	*Edge stabilization for the generalized Stokes problem: a continuous interior penalty method* Erik Burman and Peter Hansbo
2003–17	*A conservative flux for the continuous Galerkin method based on discontinuous enrichment* Mats G. Larson and A. Jonas Niklasson

2003–18	*CAD–to–CAE integration through automated model simplification and adaptive modelling* K.Y. Lee, M.A. Price, C.G. Armstrong, M.G. Larson, and K. Samuelsson
2003–19	*Multi-adaptive time integration* Anders Logg
2003–20	*Adaptive computational methods for parabolic problems* Kenneth Eriksson, Claes Johnson, and Anders Logg
2003–21	*The FEniCS project* T. Dupont, J. Hoffman, C. Johnson, R.C. Kirby, M.G. Larson, A. Logg, and R. Scott
2003–22	*Adaptive finite element methods for LES: Computation of the mean drag coefficient in a turbulent flow around a surface mounted cube using adaptive mesh refinement* Johan Hoffman
2003–23	*Adaptive DNS/LES: a new agenda in CFD* Johan Hoffman and Claes Johnson
2003–24	*Multiscale convergence and reiterated homogenization of parabolic problem* Anders Holmbom, Nils Svanstedt, and Niklas Wellander
2003–25	*On the relationship between some weak compactnesses with different numbers of scales* Anders Holmbom, Jeanette Silfver, Nils Svanstedt, and Niklas Wellander
2003–26	*A posteriori error estimation in computational inverse scattering* Larisa Beilina and Claes Johnson
2004–01	*Computability and adaptivity in CFD* Johan Hoffman och Claes Johnson
2004–02	*Interpolation estimates for piecewise smooth functions in one dimension* Anders Logg
2004–03	*Estimates of derivatives and jumps across element boundaries for multi-adaptive Galerkin solutions of ODEs* Anders Logg
2004–04	*Multi-adaptive Galerkin methods for ODEs III: Existence and stability* Anders Logg
2004–05	*Multi-adaptive Galerkin methods for ODEs IV: A priori error estimates* Anders Logg
2004–06	*A stabilized non-conforming finite element method for incompressible flow* Erik Burman and Peter Hansbo
2004–07	*On the uniqueness of weak solutions of Navier-Stokes equations: Remarks on a Clay Institute prize problem* Johan Hoffman and Claes Johnson
2004–08	*A new approach to computational turbulence modeling* Johan Hoffman and Claes Johnson
2004–09	*A posteriori error analysis of the boundary penalty method* Kenneth Eriksson, Mats G. Larson, and Axel Mlqvist
2004–10	*A posteriori error analysis of stabilized finite element approximations of the helmholtz equation on unstructured grids* Mats G. Larson and Axel Mlqvist
2004–11	*Adaptive variational multiscale methods based on a posteriori error estimation* Mats G. Larson and Axel Mlqvist

2004–12 *Multi-adaptive Galerkin methods for ODEs V: Stiff problems*
Johan Jansson and Anders Logg

2004–13 *Algorithms for multi-adaptive time-stepping*
Johan Jansson and Anders Logg

2004–14 *Simulation of mechanical systems with individual time steps*
Johan Jansson and Anders Logg

2004–15 *Computational modeling of dynamical systems*
Johan Jansson, Claes Johnson, and Anders Logg

2004–16 *Adaptive variational multiscale methods based on a posteriori error estimation: Duality techniques for elliptic problems*
Mats G. Larson and Axel Mlqvist

2004–17 *Ultraconvergence of an interpolated finite element method for some fourth-order elliptic problems*
Andrey B. Andreev and Milena R. Racheva

2004–18 *Adaptive variational multiscale methods based on a posteriori error estimation: energy norm estimates for elliptic problems*
Mats G. Larson and Axel Mlqvist

2004–19 *Stabilized Lagrange multiplier methods for elastic contact with friction*
Per Heintz and Peter Hansbo

2005–01 *A posteriori error estimates for mixed finite element approximations of elliptic problems*
Mats G. Larson and Axel Mlqvist

2005–02 *On the numerical modeling of quasi-static crack growth in linear elastic fracture mechanics*
Per Heintz

These preprints can be obtained from

`www.phi.chalmers.se/preprints`